Received: 2 April 2021 | Revised: 3 June 2021 | Accepted: 10 July 2021

IET Generation, Transmission & Distribution

DOI: 10.1049/gtd2.12253

The Institution of Engineering and Technology WILEY

ORIGINAL RESEARCH PAPER

A new pilot directional protection method for HVDC line based on the polarity of inductive energy

Jing Ma[1,2] | Jingya Kang[1] | Yiqing Zhou[1] | Yuchong Wu[1] | Peng Cheng[1]

[1] State Key Laboratory of Alternate Electrical Power System with Renewable Energy Sources, North China Electric Power University, Beijing 102206, China

[2] Bradley Department of Electrical and Computer Engineering, Virginia Polytechnic Institute and State University, Blacksburg, Virginia 24061, USA

Correspondence
Jing Ma, State Key Laboratory of Alternate Electrical Power System with Renewable Energy Sources, North China Electric Power University, Beijing 102206, China.
Email: hdmajing@163.com

Funding information
National Natural Science Foundation of China, Grant/Award Number: 51822703

Abstract

Concerning the poor immunity of DC line protection to fault resistance in the case of internal fault and its mal-operation proneness in the case of external fault, a new pilot directional protection scheme for HVDC line in AC/DC hybrid system based on the polarity of inductive energy is proposed. First, by analysing the conducting state of converter at different time sections, the impedance characteristic equations of converter in different commutation failure scenes are derived. On this basis, by combining the impedance characteristics of other components in DC system, the fault component network of an AC/DC hybrid system consisting of inductive impedances is established. Then, according to the difference in the flowing direction of the inductive energy in the fault component networks of internal and external faults, a protection criterion for identifying internal and external faults is constructed. Finally, simulation tests in RT-LAB verify that, the proposed method can accurately identify internal and external faults in different fault cases, unaffected by commutation failure and lightning interference and highly immune to the fault resistance. Besides, the proposed method does not involve real-time interaction of synchronous information, thus it is simple and reliable.

1 | INTRODUCTION

In recent years, HVDC transmission technology has been widely applied in new energy transmission and wide area interconnection. Since existing DC line protection often fails to operate correctly and quickly, accidents such as DC blocking and forced outage of lines occur frequently, which seriously threatens the safe and stable operation of power grid. Therefore, improving the fault response ability of DC line relay protection is very important to ensuring the stable operation of AC/DC hybrid system [1–4].

Currently, DC line protection mainly applies traveling wave protection, differential under-voltage protection and pilot current differential protection schemes [5, 6]. Traveling wave protection uses information such as the polarity and amplitude of the initial traveling wave after fault occurs to form the protection criterion. Due to its super-fast operation characteristic, this protection method has become one of the primary protection schemes for DC line [7]. However, in real operation, in order to avoid the influence of external metallic fault, traveling wave protection has relatively high setting value, thus it may fail to identify internal high-resistance fault. In addition, traveling wave protection needs to set the operation value through simulation tests, and it has poor immunity to lightning interference and high requirements for protection devices [8–10]. Differential under-voltage protection constitutes the protection principle by detecting the voltage differential value and voltage amplitude level. It is one of the primary protection schemes for DC line, but it also serves as backup protection of traveling wave protection. Compared with traveling wave protection, differential under-voltage protection is more sensitive and reliable. However, in real operation, differential under-voltage protection also has poor immunity to the fault resistance, and needs to set the operation value through simulation tests. Pilot current differential protection uses the sum of currents on two line ends to construct the protection criterion, which can clear high-resistance fault that escapes traveling wave protection and differential under-voltage protection [11, 12]. However, in real operation, in order to avoid interferences such as external AC-side fault, the operation delay of pilot current differential protection may reach 1100 ms in the worst case, thus it cannot serve as backup protection for DC line [13].

Besides, pilot current differential protection involves real-time exchange of electrical information on two line ends, thus it has higher requirements for the communication channel and data synchronicity.

Since DC line protection requires high operation speed, and protection schemes based on fault transient component can greatly shorten the operation time, transient-based protection has become one of the main focuses of research on DC line protection. Ref. [4] formed the transient protection criterion according to the difference in high-frequency and low-frequency contents of voltage and current at the relaying point in case of internal and external faults. However, transient-based protection has high sampling frequency, thus it is vulnerable to high-frequency interferences such as lightning interference. Ref. [14] proposed a protection scheme based on the similarity between transient current waveforms on two line ends, which is not affected by the inverter power supply. However, this method involves the interaction of electrical information on two line ends, thus it has higher requirement for the communication device, and fault identification is affected by data synchronization error.

Currently available DC line pilot directional protection methods mainly include the traveling wave based pilot directional protection and the transient based pilot directional protection. (1) The traveling wave based pilot directional protection method [15–17] constructs the protection criterion according to the characteristics of the forward and backward traveling waves. This method is poorly immune to the fault resistance and lacks the reference for protection setting. The proposed protection criterion is based on the impedance characteristic of the non-fault area, which is not affected by the fault line. Thus the proposed method is better immune to the fault resistance. Besides, the proposed method adopts an adaptive criterion as the reference for protection setting. (2) The transient based pilot directional protection method [18] utilizes the high-frequency components in the fault information to form the protection criterion. This method uses a high sampling frequency, and does not consider the effect of commutation failure on the protection. The proposed method uses the sampling frequency of 10 kHz, which is the same as in the engineering practice. Meanwhile, the proposed method constructs the protection criterion by considering the impedance characteristic equations of the converter under different commutation failure conditions and combining the impedance characteristics of other components. Thus, the proposed method eliminates the effect of commutation failure on the protection fundamentally.

In view of the above problems, a new pilot directional protection principle for HVDC line based on the polarity of inductive energy is proposed. The remainder of this paper is organized as follows. In Section 2, the impedance characteristic equations of converter in different commutation failure scenes are derived, and the fault component network of AC/DC hybrid system consisting of inductive impedances is built. Then, according to different flowing directions of inductive energy in the fault component networks of internal and external faults, a protection criterion is constructed for the identification of internal and external faults in Section 3. In Section 4, the simulation model is built and hardware-in-loop tests are conducted to verify the effectiveness of the proposed method. Finally, concluding remarks are presented in Section 5. Compared with existing DC line protection schemes, the proposed method has the following advantages: (a) it can identify internal faults with high fault resistance correctly and reliably, unaffected by the distribution capacitance of DC line and the commutation failure. (b) It does not require the transmission of real-time electrical information, so it has low demand on the communication bandwidth. (c) It is not affected by the lightning interference due to its low sampling frequency. (d) It includes a complete setting procedure, thus the operation values need not be set through simulation tests.

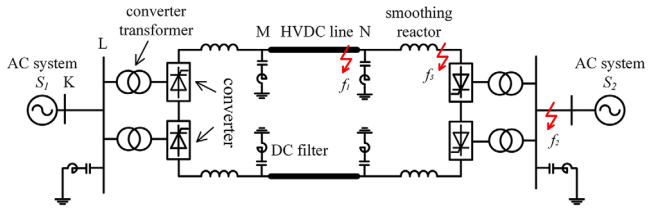

FIGURE 1 AC/DC hybrid system

2 | IMPEDANCE CHARACTERISTIC EQUATIONS OF DIFFERENT COMPONENTS IN AC/DC HYBRID SYSTEM

Take the AC/DC hybrid system shown in Figure 1 for example. It can be seen that, AC/DC hybrid system is composed of converter, DC filter, AC filter, smoothing reactor, AC system and DC line. The components on rectifier side are the same as those on inverter side, thus in this section only the impedance characteristic equations of rectifier-side components are derived.

2.1 | Impedance characteristic equation of converter

In existing studies on DC line protection, inverter-side converter station is mostly taken as linear time-invariant system and is equalized to a constant impedance in the fault component network. But in real operation, AC-side fault may result in commutation failure in DC system, which will cause inverter-side converter station to exhibit non-linear time-varying fault characteristics. Thus, equalization of inverter-side converter station to a fixed impedance is inaccurate, but different conducting states of converter should be considered.

For the AC/DC hybrid system in Figure 1, the wiring diagram of rectifier-side 12-pulse converter is shown in Figure 2 When fault occurs on DC line, rectifier-side 12-pulse converter may have the following four different conducting states.

1. Conducting state 1: VTD_1 and VTD_2 of D-bridge converter and VTY_1 and VTY_2 of Y-bridge converter are turned on;

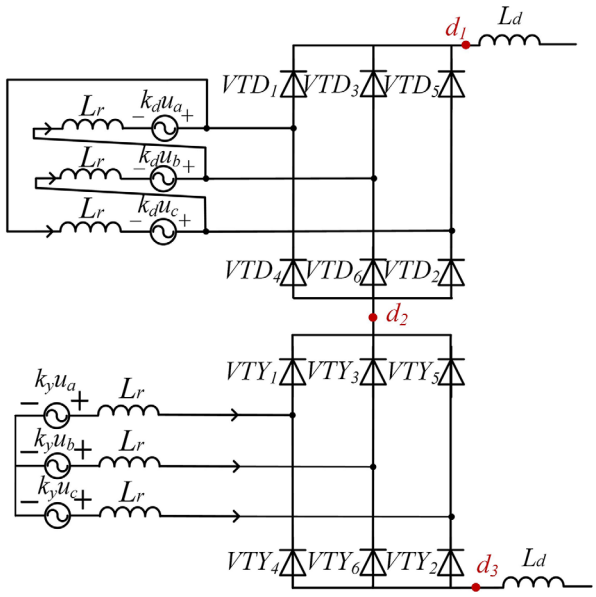

FIGURE 2 Wiring diagram of rectifier-side 12-pulse converter

2. Conducting state 2: VTD_1 and VTD_2 of D-bridge converter and VTY_1, VTY_2 and VTY_3 of Y-bridge converter are turned on;
3. Conducting state 3: VTD_1 and VTD_2 of D-bridge converter and VTY_2 and VTY_3 of Y-bridge converter are turned on;
4. Conducting state 4: VTD_1, VTD_2 and VTD_3 of D-bridge converter and VTY_2 and VTY_3 of Y-bridge converter are turned on.

When 12-pulse converter is in Conducting state 1, the following relations can be obtained from Figure 2:

$$i_{ad} = i_{bd} \tag{1}$$

$$i_{cd} + i_d = i_{bd} \tag{2}$$

$$i_{ay} = i_d \tag{3}$$

$$i_{cy} = -i_d \tag{4}$$

$$u_{d1} - L_r \frac{di_{cd}}{dt} + k_d u_c = u_d \tag{5}$$

$$u_d - L_r \frac{di_{ad}}{dt} - L_r \frac{di_{bd}}{dt} + k_d u_a + k_d u_b = u_{d1} \tag{6}$$

$$u_{d1} = k_y(u_c - u_a) - L_r \frac{di_{cy}}{dt} + L_r \frac{di_{ay}}{dt} \tag{7}$$

where u_a, u_b and u_c are three-phase voltages at rectifier-side converter bus. u_d, u_{d1} and u_{d2} are the voltages at d_1, d_2 and d_3 in Figure 2 i_{ad}, i_{bd}, i_{cd} and i_{ay}, i_{by} i_{cy} are the currents on three-phase windings of Y/△ and Y/Y converter transformers. k_y and k_d are the transformation ratios of Y/Y and Y/△ converter transformers. L_r is the inductance of converter transformer converted to the valve side. L_d is the inductance of smoothing reactor. i_d is the current flowing through the smoothing reactor.

Combining Equations (5)–(7) yields:

$$k_d u_a + k_d u_b + k_d u_c = L_r \frac{di_{ad}}{dt} + L_r \frac{di_{bd}}{dt} + L_r \frac{di_{cd}}{dt} \tag{8}$$

Since the wiring mode of converter transformer is Y/△ or Y/Y, there is no zero-sequence voltage at the converter bus when fault occurs on DC line, i.e.

$$u_a + u_b + u_c = 3u_0 = 0 \tag{9}$$

where u_0 is the zero-sequence voltage at rectifier-side converter bus.

Applying Equation (9) to (8), it can be obtained that the differentials of three-phase currents of Y/△ converter transformer satisfy the following equation:

$$0 = L_r \frac{di_{ad}}{dt} + L_r \frac{di_{bd}}{dt} + L_r \frac{di_{cd}}{dt} \tag{10}$$

Thus according to Equations (1), (2) and (10), three-phase currents of Y/△ converter transformer can be calculated:

$$\begin{cases} i_{ad} = i_{bd} = \dfrac{1}{3} i_d \\ i_{cd} = -\dfrac{2}{3} i_d \end{cases} \tag{11}$$

Combining Equations (5)–(7) and (11) yields:

$$-k_y u_a + \frac{8}{3} L_r \frac{di_d}{dt} + (k_d + k_y) u_c = u_d \tag{12}$$

According to Figure 1, three-phase voltages at the converter bus and three-phase currents on AC line L-K are respectively:

$$\begin{cases} u_a = r_1 i_a + l_1 \dfrac{di_a}{dt} + e_{sa} \\ u_b = r_1 i_b + l_1 \dfrac{di_b}{dt} + e_{sb} \\ u_c = r_1 i_c + l_1 \dfrac{di_c}{dt} + e_{sc} \end{cases} \tag{13}$$

$$\begin{cases} i_a = -k_d i_{ad} - k_y i_{ay} + C_a \\ i_b = -k_d i_{bd} - k_y i_{by} + C_b \\ i_c = -k_d i_{cd} - k_y i_{cy} + C_c \end{cases} \tag{14}$$

where r_1 and l_1 are the positive-sequence resistance and inductance of AC line L-K. e_{sa}, e_{sb} and e_{sc} are the equivalent three-phase emfs of AC system S1. C_a, C_b and C_c are three-phase currents flowing through rectifier-side AC filter.

Combining Equations (11)–(14) yields:

$$A_1 i_d + B_1 \frac{di_d}{dt} + C_1 = u_d \tag{15}$$

where the expressions of A_1, B_1 and C_1 are respectively:

$$\begin{cases} A_1 = \left(\dfrac{k_y k_d r_1}{3} + k_y k_y r_1\right) + (k_d + k_y)\left(k_d r_1 \dfrac{2}{3} + k_y r_1\right) \\ B_1 = \left(\dfrac{k_y k_d l_1}{3} + k_y k_y l_1\right) + \frac{8}{3} L_r + (k_d + k_y)(k_d l_1 \dfrac{2}{3} + k_y l_1) \\ C_1 = -k_y r_1 C_a - k_y l_1 \dfrac{dC_a}{dt} - k_y e_{sa} + (k_d + k_y) r_1 C_c \\ \quad + (k_d + k_y) l_1 \dfrac{dC_c}{dt} + (k_d + k_y) e_{sc} \end{cases} \tag{16}$$

It can be seen from Equation (16) that, A_1 is affected by the resistance AC line; B_1 is affected by the equivalent inductance of converter and the inductance of AC line; C_1 is affected by the current flowing through AC filter and three-phase voltages of AC system. Therefore, in the fault component network of DC line fault, the equivalent inductance of converter in Conducting state 1 is $8L_r/3$, and the impedance characteristic equation of converter in Conducting state 1 is:

$$Z_{op1} = j\frac{8}{3} w L_r \tag{17}$$

where w is the angular frequency.

Similarly, the impedance characteristic equations of converter in the other conducting states can be derived:

$$\begin{cases} Z_{op2} = j\dfrac{13}{6} w L_r \\ Z_{op3} = j\dfrac{8}{3} w L_r \\ Z_{op4} = j\dfrac{5}{2} w L_r \end{cases} \tag{18}$$

where Z_{op2}, Z_{op3} and Z_{op4} are the impedances of converter in Conducting state 2, Conducting state 3 and Conducting state 4.

The conducting states of the inverter-side converter under commutation failure conditions are listed in Table 1, where the expressions of Z_{op1}, Z_{op2}, Z_{op3} and Z_{op4} are shown in Equations (17) and (18).

According to Table 1, when commutation failure occurs, the inverter-side converter still operates in Conducting state 1, 2, 3 or 4. Thus the impedance characteristic equations of the converter are still those shown in Equations (17) and (18).

TABLE 1 Conducting states of the inverter-side converter under commutation failure conditions

	Initial conducting state	Conducting state after receiving the firing angle	Conducting state after commutation failure
Conducting state	Conducting state 1	Conducting state 2	Conducting state 1
Impedance characteristic equation	Z_{op1}	Z_{op2}	Z_{op1}
Conducting state	Conducting state 2	Conducting state 2	Conducting state 1
Impedance characteristic equation	Z_{op2}	Z_{op2}	Z_{op1}
Conducting state	Conducting state 3	Conducting state 4	Conducting state 3
Impedance characteristic equation	Z_{op3}	Z_{op4}	Z_{op3}
Conducting state	Conducting state 4	Conducting state 4	Conducting state 3
Impedance characteristic equation	Z_{op4}	Z_{op4}	Z_{op3}

2.2 | Impedance characteristic equations of other components

2.2.1 | Impedance characteristic equation of DC filter

For AC/DC hybrid system in Figure 1, the network structure of rectifier-side DC filter is shown in Figure 3, where C_1, C_2, L_1 and L_2 are the structural parameters of DC filter.

According to Figure 3, the impedance characteristic equation of DC filter can be obtained:

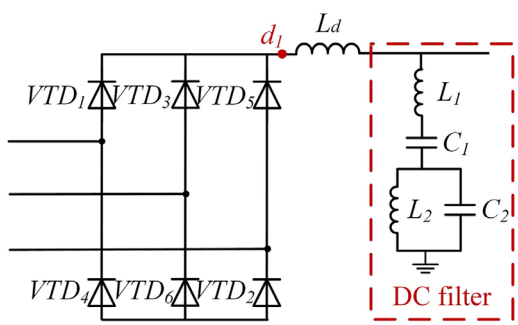

FIGURE 3 Network structure of DC filter

$$Z_{dc} = j(wL_1 - \frac{1}{wC_1} + \frac{wL_2}{1 - w^2 C_2 L_2}) \tag{19}$$

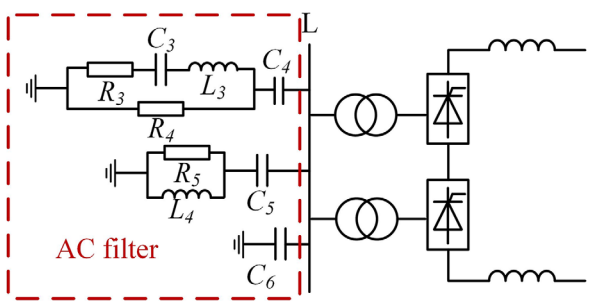

FIGURE 4 Network structure of AC filter

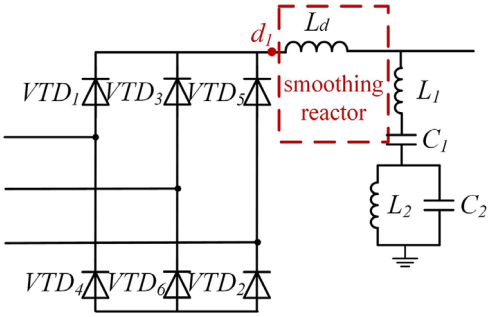

FIGURE 5 Network structure of smoothing reactor

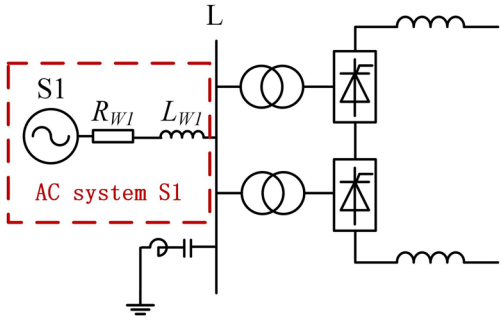

FIGURE 6 Network structure of rectifier-side AC system

2.2.2 | Impedance characteristic equation of AC filter

The network structure of rectifier-side AC filter is shown in Figure 4, where C_3, C_4, C_5, C_6, R_3, R_4, R_5, L_3 and L_4 are the structural parameters of AC filter.

According to Figure 4, the impedance characteristic equation of AC filter can be obtained:

$$\begin{cases} Z_{ac} = Z_{ac1}//Z_{ac2}//Z_{ac3} \\ Z_{ac1} = -j\dfrac{1}{wC_6} \\ Z_{ac2} = \dfrac{w^2R_5L_4^2 + jwR_5^2L_4}{R_5^2 + w^2L_4^2} - j\dfrac{1}{wC_5} \\ Z_{ac3} = \dfrac{(R_3 + jwL_3 - j\frac{1}{wC_3}) * R_4}{R_3 + jwL_3 - j\frac{1}{wC_3} + R_4} - j\dfrac{1}{wC_4} \end{cases} \tag{20}$$

2.2.3 | Impedance characteristic equation of smoothing reactor

The network structure of rectifier-side smoothing reactor is shown in Figure 5

According to Figure 5, the impedance characteristic equation of smoothing reactor can be obtained:

$$Z_d = jwL_d \tag{21}$$

2.2.4 | Impedance characteristic equation of rectifier-side AC system

The network structure of rectifier-side AC system is shown in Figure 6, where R_{W1} and L_{W1} are the equivalent resistance and inductance of rectifier-side AC system.

According to Figure 6, the impedance characteristic equation of rectifier-side AC system S1 can be obtained:

$$Z_{s1} = R_{W1} + jwL_{W1} \tag{22}$$

2.3 | Impedance characteristic equation of rectifier side of AC/DC hybrid system

According to Figure 1, when a fault occurs on DC line, the impedance of the rectifier side is formed in the following way. The impedance of AC system Z_{s1} is connected in parallel with the impedance of AC filter Z_{ac}, the result of which is connected in series with the converter impedance Z_c and the impedance of smoothing reactor Z_d, the result of which is then connected in parallel with the impedance of DC filter Z_{dc}. Therefore, when deriving the impedance equation of the rectifier side, the parallel impedance of Z_{s1} and Z_{ac} is calculated first:

$$\begin{aligned} Z_{rec1} &= Z_{s1}//Z_{ac} \\ &= (R_{W1} + jwL_{W1})//\left(-j\frac{1}{wC_6}\right) \\ &\quad //\left(\frac{w^2R_5L_4^2 + jwR_5^2L_4}{R_5^2 + w^2L_4^2} - j\frac{1}{wC_5}\right) \\ &\quad //\left(\frac{(R_3 + jwL_3 - j\frac{1}{wC_3}) \times R_4}{R_3 + jwL_3 - j\frac{1}{wC_3} + R_4} - j\frac{1}{wC_4}\right) \end{aligned} \tag{23}$$

In Equation (23), the only variable is w, and the other parameters are all constants. Then, the series impedance of Z_{rec1}, Z_c and Z_d is calculated. Finally, the parallel impedance of this series impedance and Z_{dc} is calculated, so that the impedance characteristic equation of the rectifier side is obtained:

$$\begin{aligned} Z_{rec} &= (Z_{s1}//Z_{ac} + Z_d + Z_c)//Z_{dc} \\ &= j\frac{a_{13}w^{13} + a_{11}w^{11} + \cdots + a_1w}{a_{12}w^{12} + a_{10}w^{10} + \cdots + a_0} \end{aligned} \tag{24}$$

where a_{13}, a_{12}, a_{11}, a_{10}, a_9, a_8, a_7, a_6, a_5, a_4, a_3, a_2, a_1 and a_0 are constants calculated according to the parameters of different components. Both a_{13} and a_{12} are above 0.

According to Equation (24), the impedance of rectifier side of AC/DC hybrid system Z_{rec} can be inductive or capacitive, depending on the value of angular frequency w.

2.3.1 | When Z_{rec} is inductive

For real-time calculation of Equation (24) in the inductive frequency band, Z_{rec} is only the function of w. However, it can be seen from Equations (17) and (18) that, the impedance characteristic equation of converter is time-varying. Since the fault may occur at any time, how the impedance characteristics of converter in different conducting states affect the impedance characteristic of rectifier side should be considered.

According to Equation (24), the smaller the inductance of converter is, the weaker the inductive characteristic of Z_{rec} is. Therefore, in order for Z_{rec} to be inductive in different conducting states of converter, the inductance of converter should take the minimum value, which is $13L_r/6$ according to Equations (17) and (18). In this case, the impedance of converter Z_c is $j13wL_r/6$.

Apart from the impact of impedance characteristic of converter, the transient component should be large enough in order to distinguish between internal and external faults. Since the transient component in the case of DC line fault is larger than that in normal operation state, it should be guaranteed that when DC line is normal operation state, the transient component used is large enough. The harmonic of DC line without fault is the $12k$th ($k = 1, 2, \ldots$) harmonic, and the corresponding angular frequency is $1200k\pi$rad/s. Combining Equation (24), the frequency band in which Z_{rec} is inductive can be calculated:

$$w_{hvdc} = \begin{bmatrix} \begin{pmatrix} (0 < w < w_{1.1}) \cup (w_{1.2} < w < w_{1.3}) \\ \cup (w_{1.4} < w < w_{1.5}) \cup (w_{1.6} < w < +\infty) \end{pmatrix} \cap \\ (w = 1200k\pi) \cap \\ \begin{pmatrix} (0 < w < w_{2.1}) \cup (w_{2.2} < w < w_{2.3}) \\ \cup (w_{2.4} < w < w_{2.5}) \cup (w_{2.6} < w < +\infty) \end{pmatrix} \end{bmatrix} \tag{25}$$

where $w_{1.1}$, $w_{1.2}$, $w_{1.3}$, $w_{1.4}$, $w_{1.5}$ and $w_{1.6}$ are the solutions of equation $a_{13}w^{13}+a_{11}w^{11}+\ldots+a_1w = 0$. $w_{2.2}$, $w_{2.2}$, $w_{2.3}$, $w_{2.4}$, $w_{2.5}$ and $w_{2.6}$ are the solutions of equation $a_{12}w^{12}+a_{10}w^{10}+\ldots+a_0 = 0$.

2.3.2 | When Z_{rec} is capacitive

According to Equation (25), the frequency band in which Z_{rec} is capacitive is

$$w_{hvdcC} = \begin{bmatrix} \begin{pmatrix} (w_{1.1} < w < w_{1.2}) \cup (w_{1.3} < w < w_{1.4}) \\ \cup (w_{1.5} < w < w_{1.6}) \end{pmatrix} \cap \\ (w = 1200k\pi) \cap \\ \begin{pmatrix} (w_{2.1} < w < w_{2.2}) \cup (w_{2.3} < w < w_{2.4}) \\ \cup (w_{2.5} < w < w_{2.6}) \end{pmatrix} \end{bmatrix} \tag{26}$$

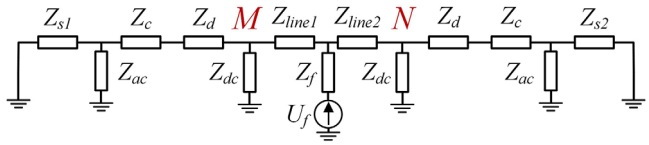

FIGURE 7 Fault component network in the case of internal fault

It can be seen from Equations (25) and (26) that, compared with the frequency band where Z_{rec} is capacitive, the frequency band where Z_{rec} is inductive is wider. Besides, the frequency band with larger transient component (i.e. the frequency band whose angular frequency is $1200k\pi$ rad/s) overlaps more with the frequency band where Z_{rec} is inductive, thus the inductive energy is larger than the capacitive energy when fault occurs. Therefore, this paper uses the fault component network consisting of inductive impedances to construct the protection criterion.

3 | DC LINE PILOT DIRECTIONAL PROTECTION PRINCIPLE BASED ON THE POLARITY OF INDUCTIVE ENERGY

3.1 | Protection scheme

3.1.1 | Internal fault

When internal fault occurs on DC line, the fault component network of AC/DC hybrid system is shown in Figure 7, where Z_{line1} is the impedance of line length between the fault point and bus M, and Z_{line2} is the impedance of line length between the fault point and bus N. Z_{s2} is the impedance of inverter-side AC system, and Z_f is the fault resistance.

According to Figure 7, the relationship between voltages and currents at bus M and bus N can be written:

$$\begin{cases} \Delta u_m = -L_m \Delta \frac{di_m}{dt} \\ \Delta u_n = -L_n \Delta \frac{di_n}{dt} \end{cases} \tag{27}$$

where L_m is the inductance of rectifier-side impedance, and L_n is the inductance of inverter-side impedance.

Thus, the energy at bus M and bus N can be defined as:

$$\begin{cases} E_m = \Delta u_m \Delta \frac{di_m}{dt} = -L_m \left(\Delta \frac{di_m}{dt} \right)^2 < 0 \\ E_n = \Delta u_n \Delta \frac{di_n}{dt} = -L_n \left(\Delta \frac{di_n}{dt} \right)^2 < 0 \end{cases} \tag{28}$$

According to Equation (28), when an internal fault occurs, the inductive energy at bus M and bus N are both smaller than 0. When the angular frequency is $w2$ or between $w1$ and $w2$ ($w1$, $w2 \in w_{hvdcL}$ and $w1 < w2$), the inductive energy at bus M and bus

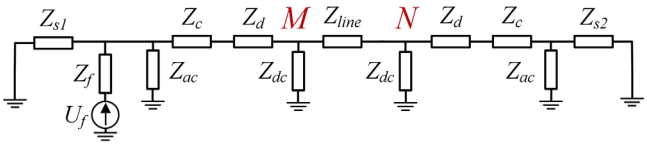

FIGURE 8 Fault component network in the case of external fault

N are:

$$\begin{cases} E_{m(w2)} = \Delta u_{m(w2)} \Delta \frac{di_{m(w2)}}{dt} = -L_{m(w2)} \left(\Delta \frac{di_{m(w2)}}{dt} \right)^2 < 0 \\ E_{n(w2)} = \Delta u_{n(w2)} \Delta \frac{di_{n(w2)}}{dt} = -L_{n(w2)} \left(\Delta \frac{di_{n(w2)}}{dt} \right)^2 < 0 \end{cases} \tag{29}$$

$$\begin{cases} E_{m(w1\sim w2)} = \Delta u_{m(w1\sim w2)} \Delta \frac{di_{m(w1\sim w2)}}{dt} = -L_{m(w1\sim w2)} \left(\Delta \frac{di_{m(w1\sim w2)}}{dt} \right)^2 < 0 \\ E_{n(w1\sim w2)} = \Delta u_{n(w1\sim w2)} \Delta \frac{di_{n(w1\sim w2)}}{dt} = -L_{n(w1\sim w2)} \left(\Delta \frac{di_{n(w1\sim w2)}}{dt} \right)^2 < 0 \end{cases} \tag{30}$$

Since the values of the inductive energy with angular frequency of *w2* are included in those with angular frequency of *w1–w2*, the combination of Equations (29) and (30) yields:

$$\begin{cases} E_{m(w1\sim w2)} < E_{m(w2)} \\ E_{n(w1\sim w2)} < E_{n(w2)} \end{cases} \tag{31}$$

where $E_{m(w1-w2)}$ and $E_{n(w1-w2)}$ are the inductive energy at bus M and bus N when the value of angular frequency is between *w1* and *w2*. $E_{m(w2)}$ and $E_{n(w2)}$ are the inductive energy at bus M and bus N when the value of angular frequency is *w2*.

3.1.2 | External fault

When external fault occurs on the rectifier side, the fault component network of AC/DC hybrid system is shown in Figure 8, where Z_{line} is the impedance of DC line.

According to the analysis in Section 1.6, the minimum value of w is $1200k\pi$; and according to ref. [19], when $w > 1200k\pi$, the impedance of DC line is inductive. In Figure 8, the relationship between voltages and currents at bus M and bus N is:

$$\begin{cases} \Delta u_m = L_m \Delta \frac{di_m}{dt} \\ \Delta u_n = -L_n \Delta \frac{di_n}{dt} \end{cases} \tag{32}$$

According to Equation (32):

$$\begin{cases} E_m = \Delta u_m \Delta \frac{di_m}{dt} = L_m \left(\Delta \frac{di_m}{dt} \right)^2 > 0 \\ E_n = \Delta u_n \Delta \frac{di_n}{dt} = -L_n \left(\Delta \frac{di_n}{dt} \right)^2 < 0 \end{cases} \tag{33}$$

Thus according to Equation (33):

$$\begin{cases} E_{m(w1\sim w2)} > E_{m(w2)} \\ E_{n(w1\sim w2)} < E_{n(w2)} \end{cases} \tag{34}$$

Combining Equations (31) and (34), the following protection criterion can be constructed:

$$S = \begin{cases} S_{rec} S_{inv} = 1 \text{ internal fault} \\ S_{rec} S_{inv} = 0 \text{ external fault} \end{cases} \tag{35}$$

where the expressions of S_{rec} and S_{inv} are respectively:

$$S_{rec} = \begin{cases} 1, \text{if}[E_{m(w1\sim w2)} < E_{m(w2)}] \\ 0, \text{if}[E_{m(w1\sim w2)} \geq E_{m(w2)}] \end{cases}$$

$$S_{inv} = \begin{cases} 1, \text{if}[E_{n(w1\sim w2)} < E_{n(w2)}] \\ 0, \text{if}[E_{n(w1\sim w2)} \geq E_{n(w2)}] \end{cases} \tag{36}$$

According to [20], the general expression of energy is the integral of the product of voltage and current:

$$E_{tra} = \int u(t) i(t) dt \tag{37}$$

where $u(t)$ is the instantaneous value of system terminal voltage; $i(t)$ is the instantaneous value of system terminal current.

As shown in Equation (27), the energy defined in this paper (E_m and E_n) is the product of the partial derivatives of voltage and current. In order to differentiate E_m and E_n from the general energy, this paper denotes E_m and E_n as the inductive energy.

3.2 | Fault start-up criterion

When fault occurs on DC line, the current flowing through DC filter rises sharply [21]. According to this feature, the following fault start-up criterion can be constructed:

$$\frac{1}{N_s} \sum_{i=1}^{N_s} I_{dc}(i) > I_{\max} \tag{38}$$

where N_s is the number of sampling points. I_{dc} is the sampling value of the current on DC filter branch. $I_{\max}$ is the threshold value.

3.3 | Pole selection criterion

According to [22], the transient component of non-fault pole is generated by electromagnetic coupling. When single-pole grounding fault occurs, fault-pole voltage drops rapidly, and the voltage of non-fault pole rises to some extent. When

double-pole short circuit fault occurs, the amplitudes of positive-pole and negative-pole voltages are basically the same. Based on this feature, the following fault pole selection criterion can be constructed:

$$\begin{cases} P \geq 1.5 & \text{positive-pole fault} \\ 0.6 < P < 1.5 & \text{double-pole fault} \\ P \leq 0.6 & \text{negative-pole fault} \end{cases} \tag{39}$$

In Equation (39), the expression of P is:

$$P = \sum_{i=1}^{N_s} \left|\Delta u_{pos}(i)\right| / \sum_{i=1}^{N_s} \left|\Delta u_{neg}(i)\right| \tag{40}$$

where $\triangle u_{pos}$ is the variation amount of positive-pole line voltage, and $\triangle u_{neg}$ is the variation amount of negative-pole line voltage.

3.4 | Impact of lightning interference

In real operation, existing DC line protection is vulnerable to lightning interference, thus the impact of lightning interference on the proposed scheme should be examined. According to Equations (35) and (36), the proposed protection criterion is based on the inductive energy corresponding to angular frequencies *w1* and *w2*, thus only lightning interferences with angular frequencies of *w1* and *w2* need to be considered.

3.4.1 | If there exists lightning voltage and current with angular frequency of *w1*

When internal fault occurs on DC line, if there exists lightning voltage and current with angular frequency of w1, there will be inductive energy $\triangle E_{m(w1)}$ and $\triangle E_{n(w1)}$ at bus M and bus N with angular frequency of *w1*. Their values can be obtained through calculation. However, each value can only be used to analyse the effect of one type of lightning interference on the protection. In order to analyse the effect of any type of lightning interference on the protection, this paper assumes that each interference component is an unknown variable. Consider that lightning voltage and current satisfy the fault component network in Figure 7, thus:

$$\begin{cases} \Delta E_{m(w1)} < 0 \\ \Delta E_{n(w1)} < 0 \end{cases} \tag{41}$$

According to Equations (31) and (41):

$$\begin{cases} E_{m(w1\sim w2)} + \Delta E_{m(w1)} < E_{m(w2)} \\ E_{n(w1\sim w2)} + \Delta E_{n(w1)} < E_{n(w2)} \end{cases} \tag{42}$$

Applying Equation (42) to (35) and (36) yields:

$$S = 1 \tag{43}$$

Thus according to Equations (35) and (43), it is identified as internal fault on DC line. The identification result of the proposed criterion is consistent with the actual fault scene.

When external fault occurs, if there exists lightning voltage and current with angular frequency of *w1*, the lightning voltage and current satisfy the fault component network in Figure 8, thus:

$$\begin{cases} \Delta E_{m(w1)} > 0 \\ \Delta E_{n(w1)} < 0 \end{cases} \tag{44}$$

According to Equations (34) and (44):

$$\begin{cases} E_{m(w1-w2)} + \Delta E_{m(w1)} > E_{m(w2)} \\ E_{n(w1-w2)} + \Delta E_{n(w1)} < E_{n(w2)} \end{cases} \tag{45}$$

Applying Equation (45) to (35) and (36) yields:

$$S = 0 \tag{46}$$

Thus according to Equations (35) and (46), it is identified as external fault. The identification result of the proposed criterion is consistent with the actual fault scene.

Based on the above analysis, even if there exists lightning voltage and current with angular frequency of *w1*, the proposed protection criterion can still identify internal and external faults correctly and reliably.

3.4.2 | If there exists lightning voltage and current with angular frequency of *w2*

When internal fault occurs on DC line, if there exists lightning voltage and current with angular frequency of *w2*, there will be inductive energy $\triangle E_{m(w2)}$ and $\triangle E_{n(w2)}$ at bus M and bus N with angular frequency of *w2*. Consider that lightning voltage and current satisfy the fault component network in Figure 7, thus:

$$\begin{cases} \Delta E_{m(w2)} < 0 \\ \Delta E_{n(w2)} < 0 \end{cases} \tag{47}$$

According to Equations (31) and (47):

$$\begin{cases} E_{m(w1-w2)} + \Delta E_{m(w2)} < E_{m(w2)} + \Delta E_{m(w2)} \\ E_{n(w1-w2)} + \Delta E_{n(w2)} < E_{n(w2)} + \Delta E_{n(w2)} \end{cases} \tag{48}$$

Applying Equation (48) to (35) and (36) yields:

$$S = 1 \tag{49}$$

Thus according to Equations (35) and (49), it is identified as internal fault on DC line. The identification result is consistent with the actual fault scene.

When external fault occurs, if there exists lightning voltage and current with angular frequency of $w2$, the lightning voltage and current satisfy the fault component network in Figure 8, thus:

$$\begin{cases} \Delta E_{m(w2)} > 0 \\ \Delta E_{n(w2)} < 0 \end{cases} \tag{50}$$

According to Equations (34) and (50):

$$\begin{cases} E_{m(w1-w2)} + \Delta E_{m(w2)} > E_{m(w2)} + \Delta E_{m(w2)} \\ E_{n(w1-w2)} + \Delta E_{n(w2)} < E_{n(w2)} + \Delta E_{n(w2)} \end{cases} \tag{51}$$

Applying Equation (51) to (35) and (36) yields:

$$S = 0 \tag{52}$$

Thus according to Equations (35) and (52), it is identified as external fault. The identification result is consistent with the actual fault scene.

Based on the above analysis, even if there exists lightning voltage and current with angular frequency of $w2$, the proposed protection criterion is still applicable.

In real operation, the frequency of lightning interference is relatively high (usually tens of kHz), while the proposed method applies relatively low sampling frequency, thus it is immune to lightning interference.

3.5 | Function of the proposed scheme after the fault

3.5.1 | Internal fault

According to Figure 7, the relationship between the voltages and currents at bus M and bus N can be written:

$$\begin{cases} \Delta u_m = -L_m \Delta \frac{di_m}{dt} \\ \Delta u_n = -L_n \Delta \frac{di_n}{dt} \end{cases} \tag{53}$$

where L_m is the inductance of rectifier-side impedance, and L_n is the inductance of inverter-side impedance.

In the case of internal fault, L_m and L_n represent the inductances of the non-fault areas, not including the inductance of DC line. Thus L_m and L_n do not vary with time, and Equation (53) still holds true. Since Equation (31) is derived from Equation (53), Equation (31) also holds true.

3.5.2 | External fault

In Figure 8, the relationship between the voltages and currents at bus M and bus N is:

$$\begin{cases} \Delta u_m = L_m \Delta \frac{di_m}{dt} \\ \Delta u_n = -L_n \Delta \frac{di_n}{dt} \end{cases} \tag{54}$$

When a rectifier-side external fault occurs, L_m is the sum of the inverter-side inductance and DC line inductance; L_n is the inverter-side inductance, not including the rectifier-side inductance. Since L_m and L_n are the inductances of the non-fault areas, they do not vary with time. Thus Equation (54) still holds true, and Equation (34) which is derived from Equation (54) also holds true.

According to the above analysis, Equation (31) remains true for internal faults, and Equation (34) remains true for external faults. Since the proposed protection criterion is based on Equations (31) and (34), the proposed scheme can continue to work after the fault.

3.6 | Sensitivity under noisy conditions

According to Equation (36), the proposed method uses the inductive energy with angular frequencies of $w2$ and $w1–w2$. Therefore, only the noise interferences with angular frequencies of $w2$ and $w1–w2$ need be considered.

3.6.1 | If there exists noise interference with angular frequency of $w1–w2$

(1) Internal fault

When an internal fault occurs on DC line and there exists a noise interference with an error of e%, the expressions of the inductive energy with angular frequencies of $w1–w2$ and $w2$ are respectively:

$$\begin{cases} E^*_{m(w1-w2)} = (1 + e(\Delta u_{m(w1-w2)}(1 + e(\Delta \frac{di_{m(w1-w2)}}{dt} \\ \quad = (1 + e(^2 E_{m(w1-w2)} \\ E^*_{n(w1-w2)} = (1 + e(\Delta u_{n(w1-w2)}(1 + e(\Delta \frac{di_{n(w1-w2)}}{dt} \\ \quad = (1 + e(^2 E_{n(w1-w2)} \end{cases} \tag{55}$$

$$\begin{cases} E^*_{m(w2)} = E_{m(w2)} \\ E^*_{n(w2)} = E_{n(w2)} \end{cases} \tag{56}$$

According to Equation (55):

$$\begin{cases} E^*_{m(w1-w2)} = (1 + e(^2 E_{m(w1-w2)} \\ \quad = (1 + e(^2 E_{m(w1)} + (1+e(^2 E_{m(w2)} + (1+e(^2 E_{mp} \\ E^*_{n(w1-w2)} = (1 + e(^2 E_{n(w1-w2)} \\ \quad = (1 + e(^2 E_{n(w1)} + (1+e(^2 E_{n(w2)} + (1+e(^2 E_{np} \end{cases} \tag{57}$$

where E_{mp} is the inductive energy at bus M with angular frequency of *w1–w2* (not including the angular frequencies of *w1* and *w2*); E_{np} is the inductive energy at bus N with angular frequency of *w1–w2* (not including the angular frequencies of *w1* and *w2*).

Combining Equations (56) and (57) yields:

$$\begin{cases} E^*_{m(w1-w2)} - E^*_{m(w2)} = (1+e(^2 E_{m(w1)} + (1+e(^2 E_{m(w2)} + (1+e(^2 E_{mp} - E_{m(w2)} \\ \quad = \underbrace{(1+e(^2 E_{m(w1)} + (e^2+2e(E_{m(w2)}}_{E_A} + \underbrace{(1+e(^2 E_{mp}}_{E_B} \\ E^*_{n(w1-w2)} - E^*_{n(w2)} = (1+e(^2 E_{n(w1)} + (1+e(^2 E_{n(w2)} + (1+e(^2 E_{np} - E_{n(w2)} \\ \quad = \underbrace{(1+e(^2 E_{n(w1)} + (1+e(^2 E_{n(w2)}}_{E_C} + \underbrace{(1+e(^2 E_{np}}_{E_D} \end{cases} \tag{58}$$

For E_A and E_C in Equation (58), [23] pointed out that when the angular frequency is $1200k\pi$, the differentials of DC line voltage and current decrease as k increases. According to Equation (25), *w1* and *w2* both fall in the interval of $1200k\pi$, and $w1<w2$. Thus $|u_{m(w1)}| > |u_{m(w2)}|$, $|\triangle di_{m(w1)}/dt| > |\triangle di_{m(w2)}/dt|$, $|u_{n(w1)}| > |u_{n(w2)}|$ and $|\triangle di_{n(w1)}/dt| > |\triangle di_{n(w2)}/dt|$, which combined with Equation (28) yield:

$$\begin{cases} E_{m(w1)} < E_{m(w2)} < 0 \\ E_{n(w1)} < E_{n(w2)} < 0 \end{cases} \tag{59}$$

Consider that $(1+e)^2 > 0$ and $(1+e)^2 > e^2+2e$, combining Equations (58) and (59) yields:

$$\begin{cases} E_A = (1 + e(^2 E_{m(w1)} + (e^2 + 2e(E_{m(w2)} < 0 \\ E_C = (1 + e(^2 E_{n(w1)} + (e^2 + 2e(E_{n(w2)} < 0 \end{cases} \tag{60}$$

For E_B and E_D in Equation (58): according to Equation (28), the inductive energy at bus M and bus N in the case of internal fault are both below 0, thus $E_B < 0$ and $E_D < 0$.

Hence, E_A, E_B, E_C and E_D are all smaller than 0. According to Equation (58):

$$\begin{cases} E^*_{m(w1-w2)} - E^*_{m(w2)} < 0 \\ E^*_{n(w1-w2)} - E^*_{n(w2)} < 0 \end{cases} \tag{61}$$

Applying Equation (61) to (35) and (36) yields:

$$S = 1 \tag{62}$$

Referring to Equations (35) and (62), the protection will identify it as an internal fault, which is correct.

(2) External fault

When an external fault occurs and there exists a noise interference with an error of e%, the expressions of the inductive energy with angular frequencies of *w1–w2* and *w2* are respectively:

$$\begin{cases} E^*_{m(w1-w2)} = (1 + e(\Delta u_{m(w1-w2)} \left(1 + e\left(\Delta \frac{di_{m(w1-w2)}}{dt}\right.\right. \\ \quad = (1 + e(^2 E_{m(w1-w2)} \\ E^*_{n(w1-w2)} = (1 + e(\Delta u_{n(w1-w2)} \left(1 + e\left(\Delta \frac{di_{n(w1-w2)}}{dt}\right.\right. \\ \quad = (1 + e(^2 E_{n(w1-w2)} \end{cases} \tag{63}$$

$$\begin{cases} E^*_{m(w2)} = E_{m(w2)} \\ E^*_{n(w2)} = E_{n(w2)} \end{cases} \tag{64}$$

According to Equation (63):

$$\begin{cases} E^*_{m(w1-w2)} = (1 + e(^2 E_{m(w1-w2)} \\ = (1 + e(^2 E_{m(w1)} + (1 + e(^2 E_{m(w2)} + (1 + e(^2 E_{mp} \\ E^*_{n(w1-w2)} = (1 + e(^2 E_{n(w1-w2)} \\ = (1 + e(^2 E_{n(w1)} + (1 + e(^2 E_{n(w2)} + (1 + e(^2 E_{np} \end{cases} \tag{65}$$

Combining Equations (64) and (65) yields:

$$\begin{cases} E^*_{m(w1-w2)} - E^*_{m(w2)} \\ = (1 + e(^2 E_{m(w1)} + (1 + e(^2 E_{m(w2)} + (1 + e(^2 E_{mp} - E_{m(w2)} \\ \quad = \underbrace{(1 + e(^2 E_{m(w1)} + (e^2 + 2e(E_{m(w2)}}_{E_A} + \underbrace{(1 + e(^2 E_{mp}}_{E_B} \\ E^*_{n(w1-w2)} - E^*_{n(w2)} \\ = (1 + e(^2 E_{n(w1)} + (1 + e(^2 E_{n(w2)} + (1 + e(^2 E_{np} - E_{n(w2)} \\ \quad = \underbrace{(1 + e(^2 E_{n(w1)} + (1 + e(^2 E_{n(w2)}}_{E_C} + \underbrace{(1 + e(^2 E_{np}}_{E_D} \end{cases} \tag{66}$$

For E_A and E_C in Equation (66), [23] pointed out that when the angular frequency is $1200k\pi$, the differentials of DC line voltage and current decrease as k increases. According to Equation (25), *w1* and *w2* both fall in the interval of $1200k\pi$, and $w1 < w2$. Thus $|u_{m(w1)}| > |u_{m(w2)}|$, $|\triangle di_{m(w1)}/dt| > |\triangle di_{m(w2)}/dt|$, $|u_{n(w1)}| > |u_{n(w2)}|$ and $|\triangle di_{n(w1)}/dt| > |\triangle di_{n(w2)}/dt|$, which combined with Equation (33) yield:

$$\begin{cases} E_{m(w1)} > E_{m(w2)} > 0 \\ E_{n(w1)} > E_{n(w2)} > 0 \end{cases} \tag{67}$$

Consider that $(1+e)^2 > 0$ and $(1+e)^2 > e^2+2e$, combining Equations (66) and (67) yields:

$$\begin{cases} E_A = (1 + e(^2 E_{m(w1)} + (e^2 + 2e(E_{m(w2)} > 0 \\ E_C = (1 + e(^2 E_{n(w1)} + (e^2 + 2e(E_{n(w2)} > 0 \end{cases} \tag{68}$$

For E_B and E_D in Equation (66): according to Equation (33), the inductive energy at bus M and bus N in the case of external fault are both above 0, thus $E_B > 0$ and $E_D > 0$.

Hence, E_A, E_B, E_C and E_D are all larger than 0. According to Equation (66):

$$\begin{cases} E^*_{m(w1-w2)} - E^*_{m(w2)} > 0 \\ E^*_{n(w1-w2)} - E^*_{n(w2)} > 0 \end{cases} \tag{69}$$

Applying Equation (69) to (35) and (36) yields:

$$S = 0 \tag{70}$$

Referring to Equations (35) and (70), the protection will correctly identify it as an external fault.

3.6.2 | If there exists noise interference with angular frequency of *w2*

Since the inductive energy with angular frequency of *w2* is included in the inductive energy with angular frequency of *w1*–*w2*, when there exists noise interference with angular frequency of *w2*, an interference component will be added to both sides of Equations (31) and (34). Thus the inequalities in Equations (31) and (34) still hold true, and the protection criterion is still applicable.

According to the above analysis, the proposed method can identify internal and external faults correctly and reliably even when there is noise interference.

4 | SIMULATION VERIFICATION

4.1 | Test system

In order to verify the feasibility and effectiveness of the proposed scheme, simulation tests are conducted in RT-LAB experimental platform shown in Figure 9 The structure of AC/DC hybrid system is shown in Figure 1, and its main parameters are shown in Table 2 By applying the parameters of different components to (24) and (25), it can be calculated that the minimum angular frequency for the system to be inductive is 1200π rad/s, thus *w1* is set to be 1200π rad/s, and *w2* is set to be 2400π rad/s. The fault is set to occur at $t = 0$ s.

The higher the sampling frequency is, the more data can be collected. But a high sampling frequency means a high demand on the sampling device and a large computation amount. To compromise, the sampling frequency of the proposed scheme is set at 10 kHz.

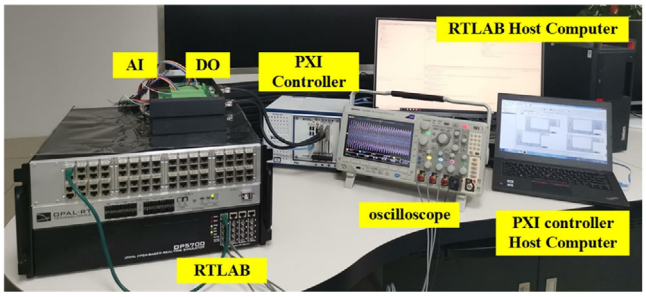

FIGURE 9 RT-LAB test platform

TABLE 2 Main parameters of AC/DC hybrid system

Parameter name	Parameter value	Parameter name	Parameter value
L_d	290 mH	C_5	6.685 μF
Positive-sequence resistance of AC line	0.0216 Ω/km	C_6	3.342 μF
Positive-sequence reactance of AC line	0.2750 Ω/km	L_1	9.847 mH
Zero-sequence resistance of AC line	0.1672 Ω/km	L_2	582.95 mH
Zero-sequence reactance of AC line	0.6255 Ω/km	L_3	136.4 mH
C_1	1.05 μF	L_4	13.6 mH
C_2	3.286 μF	R_3	29.76 Ω
C_3	74.28 μF	R_4	261.87 Ω
C_4	6.685 μF	R_5	83.32 Ω

4.2 | Internal fault on DC line with different fault resistances

Suppose fault occurs at the midpoint of positive-pole DC line via different fault resistances, the variation curves of $[E_{m(w1-w2)} - E_{m(w2)}]$ and $[E_{n(w1-w2)} - E_{n(w2)}]$ are shown in Figure 10.

It can be seen from Figure 10(a) and (b) that, as the fault resistance increases, the values of $[E_{m(w1-w2)} - E_{m(w2)}]$ and $[E_{n(w1-w2)} - E_{n(w2)}]$ at the same time section both keep increasing. Applying the values of $[E_{m(w1-w2)} - E_{m(w2)}]$ and $[E_{n(w1-w2)}$

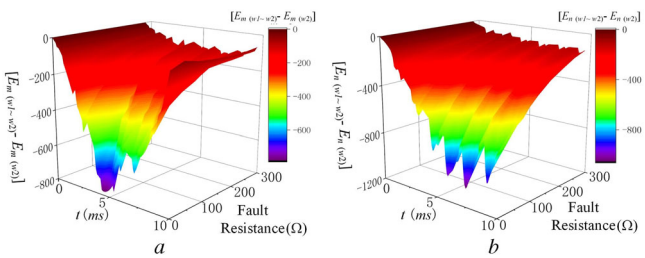

FIGURE 10 Variation curve of $[E_{m(w1-w2)} - E_{m(w2)}]$ and $[E_{n(w1-w2)} - E_{n(w2)}]$ when internal fault occurs with different fault resistances. (a) Variation curve of $[E_{m(w1-w2)} - E_{m(w2)}]$ when internal fault occurs with different fault resistances,(b) variation curve of $[E_{n(w1-w2)} - E_{n(w2)}]$ when internal fault occurs with different fault resistances

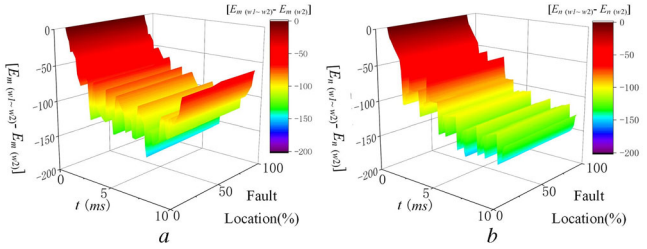

FIGURE 11 Variation curve of $[E_{m(w1-w2)} - E_{m(w2)}]$ and $[E_{n(w1-w2)} - E_{n(w2)}]$ when fault occurs at different locations on DC line, (a) Variation curve of $[E_{m(w1-w2)} - E_{m(w2)}]$ when fault occurs at different locations on DC line,(b) Variation curve of $[E_{n(w1-w2)} - E_{n(w2)}]$ when fault occurs at different locations on DC line

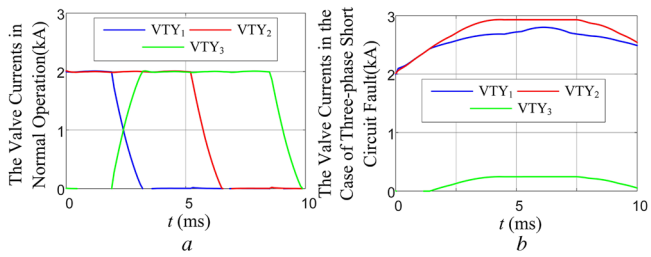

FIGURE 12 Valve currents of inverter-side Y-bridge converter: (a) Valve currents of Y-bridge converter in normal operation state, (b) valve currents of Y-bridge converter in the case of three-phase short circuit fault

$- E_{n(w2)}]$ to Equations (35) and (36) yields: $S = 1$, thus the fault is identified to be internal fault on DC line. According to Figure 10(a), the maximum value of $[E_{m(w1-w2)} - E_{m(w2)}]$ is -149.11, which appears at $t = 4.5$ ms when the fault resistance is 300 Ω. And according to Figure 10(b), the maximum value of $[E_{n(w1-w2)} - E_{n(w2)}]$ is -151.54, which appears at $t = 6.9$ ms when the fault resistance is 300 Ω. Therefore, the proposed method is proved to be highly sensitive to high-resistance fault on DC line.

4.3 | Fault at different locations on DC line

Suppose fault occurs at different locations on negative-pole DC line via fault resistance of 300 Ω, the variation curves of $[E_{m(w1-w2)} - E_{m(w2)}]$ and $[E_{n(w1-w2)} - E_{n(w2)}]$ are shown in Figure 11.

According to Figure 11(a) and (b), as the fault location varies, the values of $[E_{m(w1-w2)} - E_{m(w2)}]$ and $[E_{n(w1-w2)} - E_{n(w2)}]$ at the same time section both fluctuate very slightly. Applying the values of $[E_{m(w1-w2)} - E_{m(w2)}]$ and $[E_{n(w1-w2)} - E_{n(w2)}]$ to Equations (35) and (36) yields: $S = 1$, thus it is identified as internal fault on DC line. It can be seen that, when fault occurs at 10% line length from bus M, $[E_{m(w1-w2)} - E_{m(w2)}]$ has the maximum value -151.81 at $t = 7.2$ ms, and $[E_{n(w1-w2)} - E_{n(w2)}]$ has the maximum value -152.63 at $t = 6.9$ ms, which are both far below 0. Therefore, the protection criterion is not affected by the fault location, and can correctly identify high-resistance fault at the end of line.

4.4 | External fault in inverter-side AC system

Suppose three-phase short circuit fault occurs at f_2 in Figure 1, the valve currents of Y-bridge converter in the case of three-phase short circuit fault and in normal operation state are shown in Figure 12.

It can be seen from Figure 12 that, when AC/DC hybrid system is in normal operation state, the commutation from VTY_1 to VTY_3 in Y-bridge converter is finished by $t = 1.75$ ms, and VTY_2 and VTY_3 are turned on in Y-bridge converter at $t = 1.75$ ms. When three-phase short circuit fault occurs at

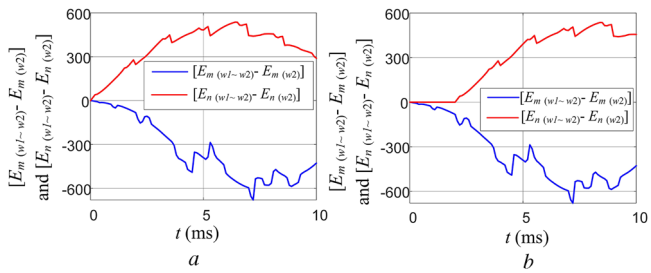

FIGURE 13 Simulation results of $[E_{m(w1-w2)} - E_{m(w2)}]$ and $[E_{n(w1-w2)} - E_{n(w2)}]$ when the data synchronization error is 0 ms/+2 ms. (a) Simulation results when the data synchronization error is 0 ms, (b) simulation results when the data synchronization error is +2 ms

f_2, VTY_1 and VTY_2 are turned on in Y-bridge converter at $t = 1.75$ ms, which means commutation fails in Y-bridge converter.

In this fault case, $E_{m(w1-w2)}$ and $E_{m(w2)}$ are both below 0, and $E_{n(w1-w2)}$ and $E_{n(w2)}$ are both above 0. According to Equations (35) and (36), $S = 0$, thus it is identified as external fault, and the protection does not operate. When the data synchronization error is 0 ms/+2 ms, the simulation results of $[E_{m(w1-w2)} - E_{m(w2)}]$ and $[E_{n(w1-w2)} - E_{n(w2)}]$ are shown in Figure 13.

According to Figure 13(a), when three-phase short circuit fault occurs at f_2, the minimum value of $[E_{m(w1-w2)} - E_{m(w2)}]$ -679.47 appears at $t = 7.2$ ms, and the maximum value of $[E_{n(w1-w2)} - E_{n(w2)}]$ 536.51 appears at $t = 6.4$ ms. It means that the fault is not on DC line, thus the protection does not operate.

According to Figure 13(b), when there is +2 ms synchronization error between inverter-side data and rectifier-side data, $[E_{n(w1-w2)} - E_{n(w2)}]$ remains above 0, thus it is first identified by inverter-side protection as backward fault. Since post-fault current switching and system restart are both completed on the rectifier side, by sending the fault direction identification result of inverter side to the rectifier side, it can be identified as external fault. Therefore, it is verified that the proposed scheme is not affected by commutation failure and data synchronization error.

TABLE 3 The maximum variation rate and variation amount of polar wave in different fault cases

Fault location	Fault resistance (Ω)	The maximum variation rate of polar wave (kV/ms)	The maximum variation amount of polar wave (kV)
	0	2588.72	252.19
f_1	100	1822.11	207.21
	300	1099.83	117.40
f_3	0	1642.19	148.23

TABLE 4 The minimum variation rate and variation amount of DC voltage in different fault cases

Fault location	Fault resistance (Ω)	The minimum variation rate of DC voltage (kV/ms)	The minimum variation amount of DC voltage (kV)
	0	−1650.37	−124.26
f_1	100	−1582.68	−54.71
	300	−1072.75	−52.34
f_3	0	−1526.53	−53.11

4.5 | Comparison with traveling wave protection and differential under-voltage protection

Suppose fault occurs at f_1 and f_3 in Figure 1 via different fault resistances ranging between 0 and 300 Ω, the maximum variation rate and variation amount of polar wave are shown in Table 3. The minimum variation rate and variation amount of DC voltage are shown in Table 4, and the values of $[E_{m(w1-w2)} - E_{m(w2)}]$ and $[E_{n(w1-w2)} - E_{n(w2)}]$ are shown in Table 5.

Traveling wave protection is based on the amplitude of polar wave. When the maximum variation rate and variation amount of polar wave both exceed the setting values, it is detected by traveling wave protection as internal fault on DC line. According to Table 3, when the fault resistance varies between 0 and 100 Ω, the maximum variation rate of polar wave in the case of external fault is smaller than that in the case of internal fault, and the maximum variation amount of polar wave in the case of external fault is also smaller than that in the case of internal fault. Thus traveling wave protection can correctly distinguish between internal and external faults. However, when the fault resistance varies between 100 Ω and 300 Ω, both the maximum variation rate and variation amount of polar wave in the case of external fault are larger than those in the case of internal fault, thus traveling wave protection cannot correctly distinguish between internal and external faults.

TABLE 5 Values of $[E_{m(w1-w2)} - E_{m(w2)}]$ and $[E_{n(w1-w2)} - E_{n(w2)}]$ when fault occurs at f_1 and f_3

Fault location	Fault resistance (Ω)	$[E_{m(w1-w2)} - E_{m(w2)}]$	$[E_{n(w1-w2)} - E_{n(w2)}]$
	0	−779.41	−1047.27
f_1	100	−323.36	−373.31
	300	−149.11	−151.54
f_3	0	−661.29	525.88

DC line differential under-voltage protection forms the protection criterion with the minimum variation rate and variation amount of DC voltage. When both values are smaller than the setting values, differential under-voltage protection identifies it as internal fault. According to Table 4, when the fault resistance ranges between 0 and 100 Ω, both the minimum variation rate and variation amount of DC voltage in the case of external fault are larger than those in the case of internal fault, thus differential under-voltage protection can correctly identify internal and external faults. However, when the fault resistance ranges between 100 Ω and 300 Ω, both the minimum variation rate and variation amount of DC voltage in the case of external fault are smaller than those in the case of internal fault, thus differential under-voltage protection cannot correctly identify internal and external faults.

It can be seen from Table 5 that, when fault occurs on DC line with fault resistance of 300 Ω, the values of $[E_{m(w1-w2)} - E_{m(w2)}]$ and $[E_{n(w1-w2)} - E_{n(w2)}]$ are respectively −149.11 and −151.54, both below 0. Thus according to Equations (35) and (36), it is determined by the proposed protection as internal fault. When external fault occurs with fault resistance of 0 Ω, the value of $[E_{n(w1-w2)} - E_{n(w2)}]$ is 525.88, which is far above 0. Thus it is identified as external fault, and the protection does not operate. Therefore, compared with traveling wave protection and differential under-voltage protection, the proposed method is better immune to the fault resistance.

5 | CONCLUSION

In AC/DC hybrid system, DC line protection is poorly immune to fault resistance in the case of internal fault and easily maloperates in the case of external fault. In view of these problems, a new pilot directional protection scheme for HVDC line based on the polarity of inductive energy is put forward, which has the following advantages.

1. The proposed method is not affected by the fault resistance, fault location and lightning interference, and it can identify internal and external faults correctly and reliably even when commutation failure is caused by inverter-side AC system fault.
2. The proposed method only involves the transmission of inverter-side fault direction identification result to the rectifier side, without any interaction of real-time electrical variables on two line ends, thus its requirement on the communication device is low, and the fault identification is not affected by data synchronization error.
3. The proposed method applies low sampling frequency, thus its requirement on the sampling device is low, and it is easy

to implement. Besides, the proposed protection criterion is adaptive, thus the operation values need not be set through simulation tests.

ACKNOWLEDGMENT

This work was supported by National Natural Science Foundation of China (51822703).

ORCID

Jing Ma https://orcid.org/0000-0002-8085-414X

REFERENCES

1. Wu, J.Y., et al.: An improved traveling-wave protection scheme for LCC-HVDC transmission lines. IEEE Trans. Power Del. 32(1), 106–116 (2017)
2. Zheng, Z., et al.: A transient harmonic current protection scheme for HVDC transmission line. IEEE Trans. Power Del. 27(4), 2278–2285 (2012)
3. Long, W., Nilsson, S.: HVDC transmission: Yesterday and today. IEEE Power Energy Mag. 5(2), 22–31 (2007)
4. Song, G.B., et al.: A new whole-line quick-action protection principle for HVDC transmission lines using one-end current. IEEE Trans. Power Del. 30(2), 599–607 (2015)
5. Kong, F.: Development of a novel protection device for bipolar HVDC transmission lines. IEEE Trans. Power Del. 29(5), 2270–2278 (2014)
6. Zhang, Y.K., et al.: A new protection scheme for HVDC transmission lines based on the specific frequency current of DC filter. IEEE Trans. Power Del. 34(2), 420–429 (2019)
7. Zhang, Y.: Fault analysis and traveling-wave protection scheme for bipolar HVDC lines. IEEE Trans. Power Del. 27(3), 1583–1591 (2012)
8. Guo, J.M., et al.: Global-sensitivity-based theoretical analysis and fast prediction of traveling waves with respect to fault resistance on HVDC transmission lines. IEEE Trans. Power Del. 30(4), 2007–2016 (2015)
9. Xiao, H., et al.: An improved traveling-wave protection scheme for LCC-HVDC transmission lines. IET Gener. Transm. Distrib. 11(5), 1233–1242 (2017)
10. Liu, X.L.: Real-time implementation of a hybrid protection scheme for bipolar HVDC line using FPGA. IEEE Trans. Power Del. 26(1), 101–108 (2010)
11. Kato, Y., et al.: Cable section fault detection for HVDC line protection. IEEE Trans. Power Del. 1(3), 332–336 (1986)
12. Liu, J., et al.: Transient measured impedance-based protection scheme for DC line faults in ultra high-voltage direct-current system. IET Gener. Transm. Distrib. 10(14), 3597–3609 (2016)
13. Kong, F.: Improved differential current protection scheme for CSC-HVDC transmission lines. IET Gener. Transm. Distrib. 11(4), 978–986 (2017)
14. Jia, K., et al.: Transient current waveform similarity based protection for flexible DC distribution system. IEEE Trans. Ind. Electron. 66(12), 9301–9311 (2019)
15. Wang, D., et al.: Travelling wave pilot protection for LCC-HVDC transmission lines based on electronic transformers' differential output characteristic. Int. J. Electr. Power Energy Syst. 93, 283–290 (2017)
16. Wang, D., et al.: Travelling wave directional pilot protection for hybrid HVDC transmission line. Int. J. Electr. Power Energy Syst. 115, 615–627 (2019)
17. Zheng, J., et al.: A novel pilot directional backup protection scheme based on transient currents for HVDC lines. Int. J. Electr. Power Energy Syst. 115, 105424–105424 (2020)
18. Jian, L., et al.: Transient measured impedance-based protection scheme for DC line faults in ultra high-voltage direct-current system. IET Gener. Transm. Distrib. 10(14), 3597–3609 (2016)
19. Liu, J.: Protection scheme for high-voltage direct-current transmission lines based on transient AC current. IET Gener. Transm. Distrib. 9(16), 2633–2643 (2015)
20. Leon, F.D., Cohen, J.: AC power theory from poynting theorem: Accurate identification of instantaneous power components in nonlinear-switched circuits. IEEE Trans. Power Del. 25(4), 2104–2112 (2010)
21. Mohammad, M.K.: Single-end protection algorithm for HVDC transmission lines based on the current difference. IET Gener. Transm. Distrib. 14(20), 4339–4351 (2020)
22. Dai, Z.H., et al.: A pilot protection for HVDC transmission lines based on transient energy ratio of DC filter link. IEEE Trans. Power Del. 35(4), 1695–1706 (2019)
23. Jian, L., et al.: Protection scheme for high-voltage direct-current transmission lines based on transient AC current. IET Gener. Transm. Distrib. 9(16), 2633–2643 (2015)

How to cite this article: Ma, J., et al.: A new pilot directional protection method for HVDC line based on the polarity of inductive energy. IET Gener. Transm. Distrib. 15, 3215–3228 (2021). https://doi.org/10.1049/gtd2.12253